Advances in Physics: X

ISSN: (Print) (Online) Journal homepage: www.tandfonline.com/journals/tapx20

Non-Abelian topological charge of photons in periodic/non-periodic media and non-Hermitian systems

Haedong Park, Ananya Ghatak & Sang Soon Oh

To cite this article: Haedong Park, Ananya Ghatak & Sang Soon Oh (2025) Non-Abelian topological charge of photons in periodic/non-periodic media and non-Hermitian systems, Advances in Physics: X, 10:1, 2477693, DOI: 10.1080/23746149.2025.2477693

To link to this article: https://doi.org/10.1080/23746149.2025.2477693

Published online: 01 Apr 2025.

ADVANCES IN PHYSICS: X
2025, VOL. 10, NO. 01, 1–30
https://doi.org/10.1080/23746149.2025.2477693

Taylor & Francis
Taylor & Francis Group

REVIEWS

Non-Abelian topological charge of photons in periodic/non-periodic media and non-Hermitian systems

Haedong Park[a], Ananya Ghatak[b] and Sang Soon Oh[a]

[a]School of Physics and Astronomy, Cardiff University, Cardiff, UK and [b]FORTH, IESL University of Crete, Heraklion, Greece

ABSTRACT

Multigap topology, which considers topology between more than two bands, generalizes the geometrical phase of a single band to the ones of multiple bands leading to non-Abelian band topology. While this non-Abelian band topology is normally observed for three-dimensional (3D) periodic structures such as electronic crystals, photonic crystals, and metamaterials, one- or two-dimensional (1D/2D) periodic structures can be employed with an additional dimension called 'synthetic' dimension. For the demonstration, for example, coupled optical waveguides and coupled ring resonators with phase and amplitude modulators have been employed. To observe non-Abelian nature of photon propagation, one can even employ non-periodic systems such as a finite number of coupled optical waveguides with spatially modulated couplings. Recently, the non-Abelian propagation of photons has been considered in non-Hermitian systems where gain and loss are controlled and the Bloch wave description fails. In this review, we introduce the basic concept of non-Abelian topology in different dimensions and symmetries and review recent development in the realization of non-Abelian topological charges in various physical systems such as 3D photonic crystals, metamaterials, coupled waveguides and cavity systems. Further, we discuss

ARTICLE HISTORY
Received 26 December 2024
Accepted 5 March 2025

KEYWORDS
Nodal lines; non-Abelian topological charge; quaternion numbers; photonic crystals; metamaterials

CONTACT Sang Soon Oh OhS2@cardiff.ac.uk School of Physics and Astronomy, Cardiff University, Cardiff, CF24 3AA, UK

how non-Hermiticity plays a role in the non-Abelian topology of bands or eigenvalues starting from reviewing theoretical models in condensed matter physics.

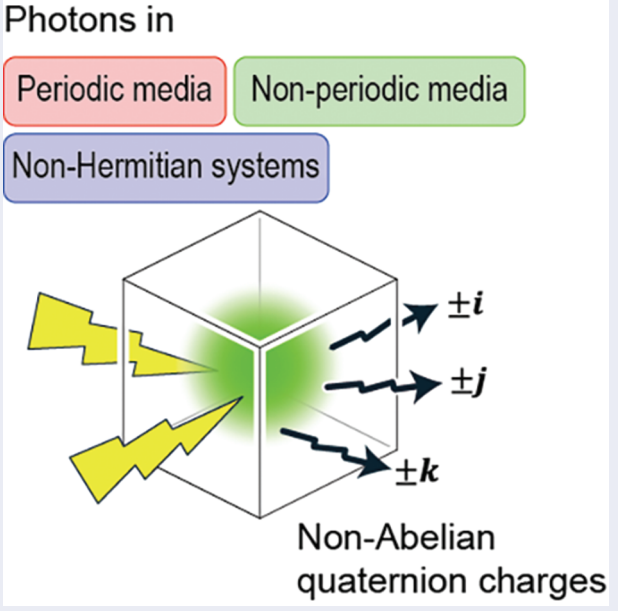

1. Introduction

Commutative relations of operators as in the addition and multiplication of integer numbers are ubiquitous in mathematics and physics forming so-called Abelian groups. Meanwhile, there are many non-commuting (including anticommuting) operators such as matrix multiplications and vector products which form non-Abelian groups. The non-commuting operators played a key role in the development of quantum mechanics, for example, the Heisenberg's uncertainty principle and Pauli and Dirac matrices. The non-Abelian group is also interesting in particle physics because it gives a foundation of the non-Abelian gauge field theory.

In the development of modern condensed matter physics in the twentieth century, the electronic band theory allowed us to describe conductors, insulators and semimetals starting from basic building blocks, e.g. lattices and unit cells of electronic crystals. In the past decades, the topological classification of electronic bands has solved the mystery of quantized conductance in quantum Hall effect and opened exciting avenues of research called topological physics in the area of electronics, electronics, photonics, and acoustics. The key concept of topological physics is the classification of topological phases with numbers, which we call topological invariants or topological charges. In general, the topological charges assigned to the electronic bands form the

group of integers $\mathbb{Z}$ or the group of integers modulo 2, $\mathbb{Z}_2$, both of which are Abelian. Also, the topological charges of nodal lines, which is the line degeneracy between two bands, forms a group of integers $\mathbb{Z}$. In multigap systems which consist of more than two bands, however, the topological charges of nodal lines, expressed by frame rotation charge, form a non-Abelian group, for example, the quaternion group $\mathbb{Q}$ for a three-band system [1]. For the last few years, the non-Abelian charge in multigap systems has been studied in photonics [2], acoustics and phonons [3]. Although the non-Abelian topological charges can be considered for electronic or photonic bands for 2D/3D periodic systems, one can consider non-Abelian holonomies in non-periodic finite systems where a state changes adiabatically, for example, in coupled waveguides [4]. Interestingly, in non-Hermitian periodic systems, the non-Abelian nature of eigenmodes can be observed in a complex energy spectrum in a shape of a braid [5].

This review will cover non-Abelian topological charges in photonic structures (photonic crystals and metamaterials) and condensed matters. Acoustic materials, synthetic dimensions, and other types of metamaterials will be excluded as they are covered by the recent review article [6]. In Section 2, we will present theoretical background to understand non-Abelian topological charges in condensed matter physics and photonics by introducing band topology together with nodal lines, frame rotation charges and Euler class. In Section 3, we review the recent work on the realization of nodal lines and Weyl points using photonic crystals and metamaterials. In Section 4, we introduce the topological invariants and the braid groups for topological description of non-Hermitian system with some experimental demonstrations and theoretical models. In Section 5, we will look at non-Abelian quantum holonomy and Thouless pumping in optical waveguides and non-Abelian topology in non-Hermitian systems.

2. Topological charges of nodal lines in three-dimensional momentum space

2.1. Brief introduction of nodal lines

A nodal line is a set of band degeneracies with a line shape in the 2D/3D momentum space. In this section, we will consider the 3D momentum space. According to their detailed shape, a number of single nodal lines are classified as straight nodal lines, nodal curves, nodal rings, nodal knots [3]. Furthermore, based on their connectivity and relative positions, a set of nodal lines (two or more) can be categorized as nodal chain(s) or nodal link(s) [3].

Similarly, in the 2D momentum space, a point degeneracy with a linear dispersion, called 'Dirac point', can exist. In many cases, a Weyl point, a point degeneracy in the 3D momentum space, is regarded as a Dirac point's counterpart in the 3D momentum space. However, they are different from each

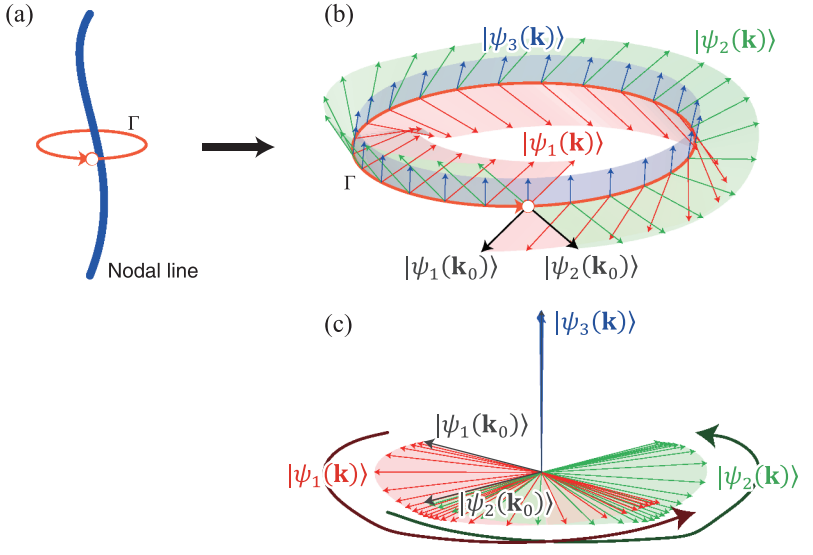

Figure 1. Illustration of the frame rotation charge (a) schematic figure of a nodal line with a closed loop Γ that encircles the nodal line. (b) Enlargement of Γ in (a) with eigenstates $|\psi_1(\mathbf{k})\rangle$, $|\psi_2(\mathbf{k})\rangle$, and $|\psi_3(\mathbf{k})\rangle$ on Γ, respectively. (c) Eigenstates in (b) moved onto the origin to plot them as if they start from the origin. The evolution of $|\psi_1(\mathbf{k})\rangle$ and $|\psi_2(\mathbf{k})\rangle$ along Γ are denoted by the dark-red and -green curved arrows, respectively. (b) and (c) are reproduced with permission from ref [7]. copyright 2022 American physical society.

other in the following two aspects. First, Dirac points can be formed when both inversion ($\mathcal{P}$) and time-reversal ($\mathcal{T}$) symmetries are satisfied, while the Weyl point is generated when one of them is broken. Second, the characterization of a Dirac point's topological invariant utilizes a closed loop around the band degeneracy, whereas the topological charges of Weyl points are calculated using a closed surface around the Weyl point. In this respect, a nodal line in the 3D momentum space shares more properties with the Dirac point rather than with the Weyl point. Specifically, nodal lines are formed when its crystal satisfies both $\mathcal{P}$ and $\mathcal{T}$ symmetries and the closed loop is also utilized to calculate a nodal line's topological charge (Figure 1a).

2.2. *Abelian and non-abelian topological charges*

Many physicists have been interested in the topological nature of nodal lines, and thus the topological quantities, called topological charges or topological invariants, have been defined and calculated. As the nodal lines share many properties with the Dirac point as mentioned earlier, one can first think of calculating Berry's phase [8], which is an Abelian charge, as a topological invariant. First, a loop is chosen so that it can enclose a band degeneracy or a set of band degeneracies (Figure 1a). Then, along the loop, eigenstates or

equivalent quantities are calculated. Finally, their evolution along the loop is analyzed by the Berry phase defined as:

$$\gamma_n = i \oint_\Gamma \langle \psi_n | \frac{\partial}{\partial k} | \psi_n \rangle dk, \tag{1}$$

where ψ_n is the eigenstate of the n-th band that is one of the two bands involved in the band degeneracies (n-th band). This method has been utilized for a Dirac point. The Berry phase, however, can be nontrivial only when the eigenstates possess imaginary components, because the Berry phase becomes always zero if the eigenstate is purely real. This can be proven from the orthogonality relation $\langle \psi_n | \psi_m \rangle = \delta_{nm}$, by differentiating with respect to k, i.e. $\partial \langle \psi_n | \psi_n \rangle / \partial k = \partial \delta_{n\,n} / \partial k$ or $\langle \partial \psi_n / \partial k | \psi_n \rangle + \langle \psi_n | \partial \psi_n / \partial k \rangle = 0$ leading to $2Re(\langle \psi_n | \partial \psi_n \partial k \rangle) = 0$. Then, this invariant cannot be utilized for a system which has a purely real eigenstate. This means that a system of nodal lines needs another topological invariant.

To address this, the Wilczek-Zee phase [9] can be applied to nodal lines. It is given by the following formula:

$$\mathbf{W} = \exp \left\{ \oint_\Gamma \mathbf{A}\,(\mathbf{k})\, dk \right\} \tag{2}$$

where

$$\mathbf{A}\,(\mathbf{k}) = A_{mn} = \left\langle \psi_m | \frac{\partial}{\partial k} | \psi_n \right\rangle \ (m < n) \tag{3}$$

is the Wilczek-Zee connection. One example of the eigenstates' distributions along the closed loop Γ around the nodal line (refer to Figure 1a) will be helpful to understand the Wilczek-Zee phase. During one winding along Γ, the net changes of direction of eigenstates ψ_n and ψ_m commonly become π (Figure 1b,c); the eigenstate's direction at the final point $\mathbf{k}_0$ after one winding becomes opposite to the eigenstate's direction at the same point $\mathbf{k}_0$ before the winding (remember that if $+\psi$ is an eigenstate of a system, $-\psi$ is considered as the equivalent to ψ). Thus, $\left\langle \psi_m | \frac{\partial}{\partial k} | \psi_n \right\rangle$ creates a non-trivial Wilczek-Zee phase. Here, we need to think about the behavior of eigenstates of other bands (not the m- or n-th bands). Unless they form any degeneracy around the degeneracy between m- and n-th bands, $\oint_\Gamma \left\langle \psi_a | \frac{\partial}{\partial k} | \psi_b \right\rangle dk$ becomes zero ($a < b < m$ or $n < a < b$).

Such properties are related to non-Abelian topological charges and invariants. One distinguishable property of a non-Abelian topological charge compared to an Abelian charge is that a topological charge contains the information about the bands making the band degeneracy in a multi-band system.

Let us assume a three-band system and formulate $A_{mn} = \left\langle \psi_m | \frac{\partial}{\partial k} | \psi_n \right\rangle$ $(m, n = 1, 2, 3)$. If a nodal line is a set of band degeneracy by the bands $m = 1$ and $n = 2$ while the third band does not contribute to the band degeneracy, the Wilczek-Zee connection is given by

$$\mathbf{A}^{12}(\mathbf{k}) = \begin{bmatrix} 0 & \left\langle \psi_1 | \frac{\partial}{\partial k} | \psi_2 \right\rangle & 0 \\ -\left\langle \psi_2 | \frac{\partial}{\partial k} | \psi_1 \right\rangle & 0 & 0 \\ 0 & 0 & 0 \end{bmatrix}. \tag{4}$$

Here, from the orthogonality $\langle \psi_n | \psi_m \rangle = \delta_{nm}$ or its derivative $\langle \partial \psi_m / \partial k | \psi_n \rangle + \langle \psi_m | \partial \psi_n / \partial k \rangle = 0$, we can derive the above skew symmetric property. All components calculated using ψ_3 become zero. Likewise, if there is another nodal line formed by the bands $m = 2$ and $n = 3$, we have the Wilczek-Zee connection $\mathbf{A}^{23}$ with $\left[\mathbf{A}^{23}\right]_{23} = \left\langle \psi_2 | \frac{\partial}{\partial k} | \psi_3 \right\rangle$, $\left[\mathbf{A}^{23}\right]_{32} = -\left\langle \psi_3 | \frac{\partial}{\partial k} | \psi_2 \right\rangle$, and 0 otherwise. The Wilczek-Zee phases $\mathbf{W}^{12} = \exp\left\{ \oint_\Gamma \mathbf{A}^{12}(\mathbf{k})\, dk \right\}$ and $\mathbf{W}^{23} = \exp\left\{ \oint_\Gamma \mathbf{A}^{23}(\mathbf{k})\, dk \right\}$, like the topological charges of nodal lines, have different non-trivial values which carry the band information.

Remarkably, we can regard the topological charges $\mathbf{W}^{12}$ and $\mathbf{W}^{23}$ as non-Abelian. This is because their relationship does not commute; $\mathbf{W}^{12}\mathbf{W}^{23} \neq \mathbf{W}^{23}\mathbf{W}^{12}$. Especially, for a three-band system, it is well known that their topological charges are written as quaternion numbers $\mathbb{Q} = \{\pm \boldsymbol{i}, \pm \boldsymbol{j}, \pm \boldsymbol{k}, \pm 1\}$ [1]. Furthermore, arithmetical calculation of multiple nodal lines can be conducted. Let us suppose a closed loop that ties a bundle of several nodal lines by the same or different pairs of bands. The non-Abelian topological charges calculated along the loop equal the multiplication of non-Abelian charges of each nodal line as we will see in the following subsection.

2.3. Properties of non-Abelian charges: phase transition, braiding, and Euler class

To understand the meaning of non-Abelian charges, we need to mention the phase transition of nodal lines. A nodal line's topological non-Abelian charge's sign may be positive or negative. If there are two nodal lines by the same pair of bands, their charges' signs may be same or opposite. If they are the same, the two nodal lines are stable so that they do not get any phase transition. Otherwise, if they are opposite, they can be pair-annihilated to form a different shape, as shown in Figure 2a via a nodal chain. From this point of view, a nodal chain can be regarded as a critical state of nodal lines' phase transition so that the states before and after the phase transition are distinguishable.

Another interesting feature of non-Abelian charges is the flipping of the charge's sign after braiding. For example, in Figure 2b, there are two nodal

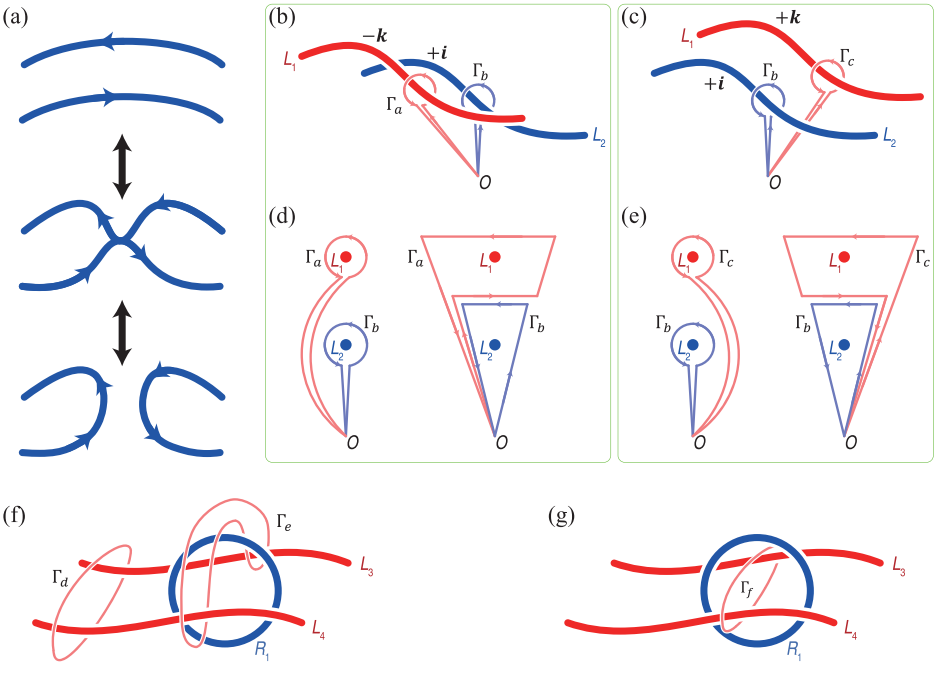

Figure 2. Schematics of nodal lines' phase transition and braiding. (a) Pair annihilation of two oppositely charged nodal lines by the same pair of bands. (b–c) Illustrations to explain the charge flipping after braiding of a nodal line. If we fix the location and charge of L_2, the charge's sign of L_1 fillips by the transition between (b) and (c). Γ_a, Γ_b, and Γ_c are closed loops to calculate the non-abelian topological charges. (d–e) configurations of nodal lines and closed loops equivalent to (b) and (c), respectively. In each panel of (d) and (e), two equivalent configurations are given. See ref. [10] to draw (b–e). The point O in (b–e) that belongs to all the closed loops is to fix the gauge of eigenstates [10,11]. (f–g) braiding of nodal lines in the viewpoint of nodal lines' stability. L_3 and L_4 are stable in (f), whereas they can be pair-annihilated in (g).

lines L_1 and L_2 that carry $-\boldsymbol{k}$ and $+\boldsymbol{i}$, respectively. These charges are calculated using the closed loops Γ_a and Γ_b, respectively. Interestingly, if we move (braid) L_1 as shown in Figure 2c, its charge becomes $+\boldsymbol{k}$. This can be explained by the closed loops' relation. The configurations of nodal lines L_1 and L_2 and closed loops Γ_a, Γ_b, and Γ_c in Figure 2b,c can be redrawn, as shown in Figure 2d,e, respectively. In each panel of Figure 2d,e, the first figures can be transformed into the second figures without changing nodal lines' any topology. The closed loops' composites in the second figures of (d) and (e) are written as $\Gamma_a \circ \Gamma_b$ and $\Gamma_b \circ \Gamma_c$, respectively, and their net loops are equal, i.e. $\Gamma_a \circ \Gamma_b = \Gamma_b \circ \Gamma_c$. By writing the relations as $\Gamma_a = \Gamma_b \circ \Gamma_c \circ \Gamma_b^{-1}$, and by substituting $+\boldsymbol{i}$, $+\boldsymbol{k}$, $-\boldsymbol{i}$ into Γ_b, Γ_c, Γ_b^{-1}, respectively, we get $-\boldsymbol{k}$ the charge of L_1 by the closed loop Γ_a.

In the above explanation, there is a critical assumption about fixing the gauge of an eigenstate. When an eigenvalue problem is solved, an eigenstate's gauge is not uniquely determined. This means $-\psi$ can also be the equivalent eigenstate if $+\psi$ is an eigenstates of a system. Although the gauge is set to be continuous in a momentum space during the calculation of a topological

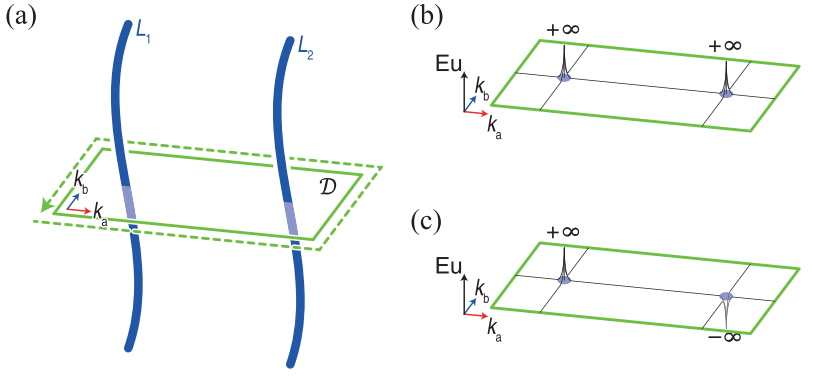

Figure 3. Illustrations about the Euler class. (a) Nodal lines L_1 and L_2 and a finite-sized patch $\mathcal{D}$ pierced by L_1 and L_2 in the three-dimensional momentum space. (b–c) example plots of the Euler form Eu when L_1 and L_2 carry non-abelian charges with (b) the same signs and (c) the opposite signs, respectively. Note that L_1 and L_2 are formed by the same pair of bands.

charge, the overall gauge should also be fixed. If not, a non-Abelian charge's sign is not determined, i.e. L_2 in Figure 2b may carry $-\boldsymbol{i}$ instead of $+\boldsymbol{i}$. Thus, to account for non-Abelian charges' braiding, we need to suppose the same gauges of all the eigenstates at O between Figure 2b–e [1,10,11].

The sign flipping with braiding can allow for the nodal lines' phase transition. The two nodal lines L_3 and L_4 in Figure 2f have the same charges by the closed loop Γ_d or Γ_e. The value is -1, and this means they are stable so that they cannot exhibit the phase transition. On the contrary, the topological charge by the loop Γ_f in Figure 2g is $+1$ so that this loop views the two nodal lines as the differently charged. The phase transition can be realized along the connectivity implied by Γ_f, as shown in Figure 2e [7,10].

To characterize the phase transition of non-Abelian charged nodal lines, a topological invariant needs to be defined, instead of a non-Abelian topological charge. The Euler class plays this role. To calculate the Euler class, we need to prepare an even number of nodal lines using the same pair of bands m and n and a finite-sized patch $\mathcal{D}$, as shown in Figure 3a. L_1 and L_2 pass through $\mathcal{D}$, i.e. the boundary $\partial\mathcal{D}$ encloses each element of L_1 and L_2. The Euler class is defined by the following formula:

$$\chi_{mn}(\mathcal{D}) = \frac{1}{2\pi}\left[\int_{\mathcal{D}} \mathrm{Eu}^{mn} dk_a dk_b - \oint_{\partial\mathcal{D}} \mathbf{a}(\mathbf{k}) \cdot d\mathbf{k}\right], \tag{5}$$

where the Euler form Eu^{mn} is given by

$$\mathrm{Eu}^{mn}(\mathbf{k}) = \langle \nabla_{\mathbf{k}} \psi^m_{\mathbf{k}} | \times | \nabla_{\mathbf{k}} \psi^n_{\mathbf{k}} \rangle, \tag{6}$$

and the Euler connection $\mathbf{a}(\mathbf{k})$ is written as

$$\mathbf{a}(\mathbf{k}) = \langle \psi^m_{\mathbf{k}} | \nabla_{\mathbf{k}} \psi^n_{\mathbf{k}} \rangle \,. \tag{7}$$

Equation 5 consists of integrals over a path $\mathcal{D}$ and along a curve $\partial\mathcal{D}$. If there is no nodal lines that pass through $\mathcal{D}$, all the two integrals become zero according to the Stokes' theorem. On the contrary, if there is the aforementioned even number of nodal lines (assuming two nodal lines), the field of the integrand Eu^{mn} possesses the singularities, and the Stokes' theorem becomes invalidated [12]. Then, the result is explained by the following correspondence between the Euler class and the non-Abelian charges (including the quaternion charges). When L_1 and L_2 carry the non-Abelian charges with same signs, the two singularities also have the same sign (see Figure 3b). This coincides with the stable nodal lines so that the nodal lines do not exhibit the phase transition. On the other hand, when the charges of L_1 and L_2 have the opposite signs, the singularities' signs become opposites (see Figure 3c), so that $\int_{\mathcal{D}} \mathrm{Eu}^{mn} dk_a dk_b$ becomes zero, and the nodal lines can be pair-annihilated like Figure 2a. In the previous section, we have mentioned about a feature of non-Abelian charges that they have the information which pair of bands makes band degeneracies in a multi-band system. Although an Euler class does not have such information explicitly, the Euler class contains the information of non-Abelian charges' signs, so that the Euler class can predict the ability of nodal lines' phase transition. It is also interesting that the Euler class does not require fixing the gauge of eigenstates which was important step of calculating the non-Abelian charges (related to Figure 2b–e). This is because the critical factor in the Euler class calculation is not the absolute but relative signs between the nodal lines.

An interesting aspect of the Euler class in this discussion is that it requires an even number of nodal lines (at least two), as shown in Figure 3a. It is natural to ask a question about the result if only one nodal line is considered when the Euler class is calculated. However, such calculations cannot generate a meaningful result. Eigenstates along a closed loop that encircles a nodal line inevitably exhibit inconsistency, referred to as the Dirac string [7,12]. However, for two nodal lines, the Dirac string can initiate and terminate at each nodal line. Then, the Dirac string can be confined in a patch $\mathcal{D}$, so that the eigenstates around $\partial\mathcal{D}$ can be smoothed. When only one nodal line pierces $\mathcal{D}$, this smoothing is impossible, so the result is not physically meaningful. Thus, to calculate the Euler class, at least two nodal lines are necessary.

3. Realization of (non-abelian charged) nodal lines using photonic crystal and metamaterials

3.1. Metallic nodal line photonic crystals

To constitute a photonic system to realize nodal lines theoretically or experimentally, metallic materials are good candidates due to their strong interaction with light via free electrons and easiness to build a complex photonic system in a macroscale. Thus, there have been many proof-of-concepts with metallic photonic systems. If we confine our interests on nodal lines, most works can be classified as (1) realization of various nodal lines and (2) phase transition of nodal lines.

The realizations of nodal lines have been conducted as the early stage studies in this field. W. Gao et al. experimentally realized a nodal ring using a cut-wire metacryatal [13]. An orthorhombic unit cell whose space group is $P4/mbm$ is placed on the $x-y$ plane. In the 3D momentum space, a nodal ring centered at the Γ-point and parallel to the $x-y$ plane is generated. Q. Yan et al. discovered a nodal chain using a 3D metallic-mesh scaffold [14]. They utilized a cubic unit cell, and the resulting nodal chain is also completely periodic along the x, y, and z-directions.

Following these experimental realizations, the main focus of the study has gradually moved to the realization of topological-phase transition of nodal lines. To this end, a given metallic photonic system needs to be tuned and the resulting nodal lines should be observed. In fact, there are only few studies that follow this story. Most studies utilize an effective analytic model instead of adjusting the structural or material parameters of a unit cell. By tuning the effective model, they theoretically prove the phase transition of nodal lines. Then, they construct the equivalent structure and observe the nodal lines (or the signs of their existence) theoretically and experimentally. For example, E. Yang et al. prepared a simple theory that considers metallic property of a photonic system. The theory has proven the phase transition of photonic nodal link based on the nodal lines' non-Abelian nature, as shown in Figure 4a. Then, their experimental work using a biaxial metal crystal exhibits the nodal link as they predicted theoretically [15].

With the increase of non-Abelian property of nodal lines, many studies have also focused on the various theoretical aspects of nodal lines. One interesting example is the discovery of a nodal point as a source or sink of non-Abelian charges. According to the conventional knowledge, when four nodal lines meet at a point, the summation of their non-Abelian charges should be zero, as displayed in Figure 4b. However, D. Wang et al. discovered that if the nodal point is at the Γ-point, the four nodal lines' directions commonly head toward (or out of) the Γ-point, as shown in Figure 4c. In other words, the nodal point acts as the sink (or source) of the non-Abelian topological charges [16].

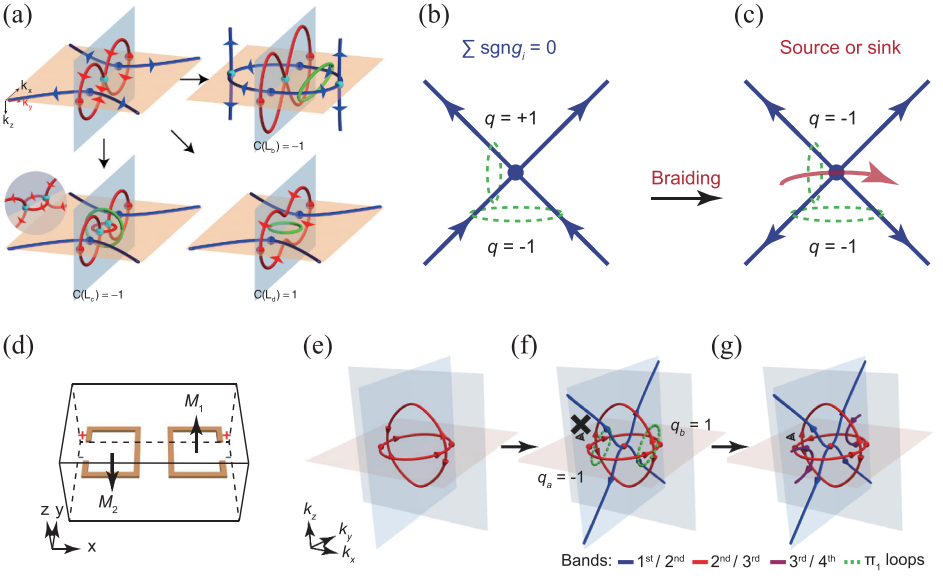

Figure 4. Examples of metallic photonic crystals for non-abelian charged nodal lines. (a) Phase transition of nodal lines based on a biaxial metallic crystal. Reprinted with permission from Ref. [15] copyright 2020 American physical society. (b-c) nodal chain whose nodal point acts as source or sink of non-abelian topological charges. (b-c) are reprinted with permission from Ref. [16] copyright 2023 American physical society. (d-g) metallic resonator (d) and the resulting four-band nodal lines (e-g). (d-g) are reprinted with permission from Ref. [17] copyright 2022 American physical society. All these utilize the frame rotation charge theory to explain the phase transition of nodal lines.

Another study considers an extra pair of bands to explain the contradiction observed in a three-band theory. The metallic resonator in Figure 4d generates the nodal lines in Figure 4e–g. The nodal lines are formed by the 1st and 2nd (the blue nodal lines), 2nd and 3rd (the red nodal rings), and 3rd and 4th bands (the purple nodal lines). With assuming only the red nodal rings, the two nodal rings' junctions satisfy the zero-sum of the non-Abelian charges, i.e. at a junction, the number of inward and outward arrows are the same (see Figure 4e). When the blue nodal lines are considered, at one junction of the two red nodal rings, all the four red nodal lines exhibit the outward directions, even though the green closed loops to calculate the non-Abelian charges are centrosymmetric with respect to the Γ-point, as shown in Figure 4f. This contradiction can be explained by regarding one more nodal lines by the pair of higher bands Figure 4g [17].

3.2. *Dielectric nodal line photonic crystals*

In a dielectric material, photonic behavior is scale-independent, i.e. when a photonic crystal grows tenfold, a photonic band structure remains with only

the eigenfrequency decreasing tenfold. This property enables a theoretical aspect of photonics to be applicable to any scale, although building a complex structure made of dielectric material is not so simple.

One of the famous realizations of a nodal line is the nodal ring by the air-gap filled double gyroid structure [18]. The double gyroid photonic crystal in Figure 5a consists of dielectric material whose refractive index is 4.0. The structure and material properties are inversion symmetric, and it has three two-fold rotation axes. Band degeneracies are formed between the 4th and 5th bands, and their set forms a nodal ring centered at the Γ-point (see Figure 5b). When it lacks the inversion symmetry, the nodal ring becomes four Weyl points, and the study in Ref. [18] mainly focuses on the Weyl points' behavior.

However, to discuss the non-Abelian topology, nodal lines by at least two different pair of bands are needed, i.e. the band structure should have at least three bands. Dielectric double diamond photonic crystal in Ref. [19] is the first example that exhibits frame rotation charges (see Figure 5c–f). The double diamond consists of two single diamonds that are counterparts to each other (see Figure 5c). Their permittivity is 16.0. The distance between the single diamonds is adjusted to break the translational symmetry by half of the lattice constant. By preserving the inversion and translational symmetry with breaking all the other symmetries, the anisotropic double diamond structure exhibits a nodal link that several nodal rings are connected infinitely in the momentum space (see Figure 5d). The bands $n = 3$, 4, and 5 participate in the generation of the nodal link. Thus, each component of the nodal link carries non-Abelian topological charges, as shown in Figure 5e–f. Each nodal line's topological charge calculated by the method in Section 2.2 is expressed as a quaternion number. If we set a loop that encloses two different nodal lines, the composite topological charge switches its sign with switching the enclose direction, as shown in Figure 5g–h.

The shape of the nodal link is determined by the double diamond's material properties (i.e. permittivity in this case) and its geometrical factors. Changing material parameters requires replacement of a given material as a new material. Thus, it is convenient to focus on the photonic crystal's geometrical deformation and observe its photonic behavior. For a double diamond dielectric photonic crystal with the permittivity of 15.0 as shown in Figure 6a, the two single diamonds' distance denoted by the green arrows is adjusted to get the structure in Figure 6b. The structure in Figure 6a bears a nodal ring which two nodal lines pass through, as shown in Figure 6d. This topology (configuration of nodal lines) gets phase transition to a nodal link, as shown in Figure 6e. Now, let us focus on the arms' thickness marked by the red dotted boxes in Figure 6b. When the thickness decreases to make Figure 6c, the

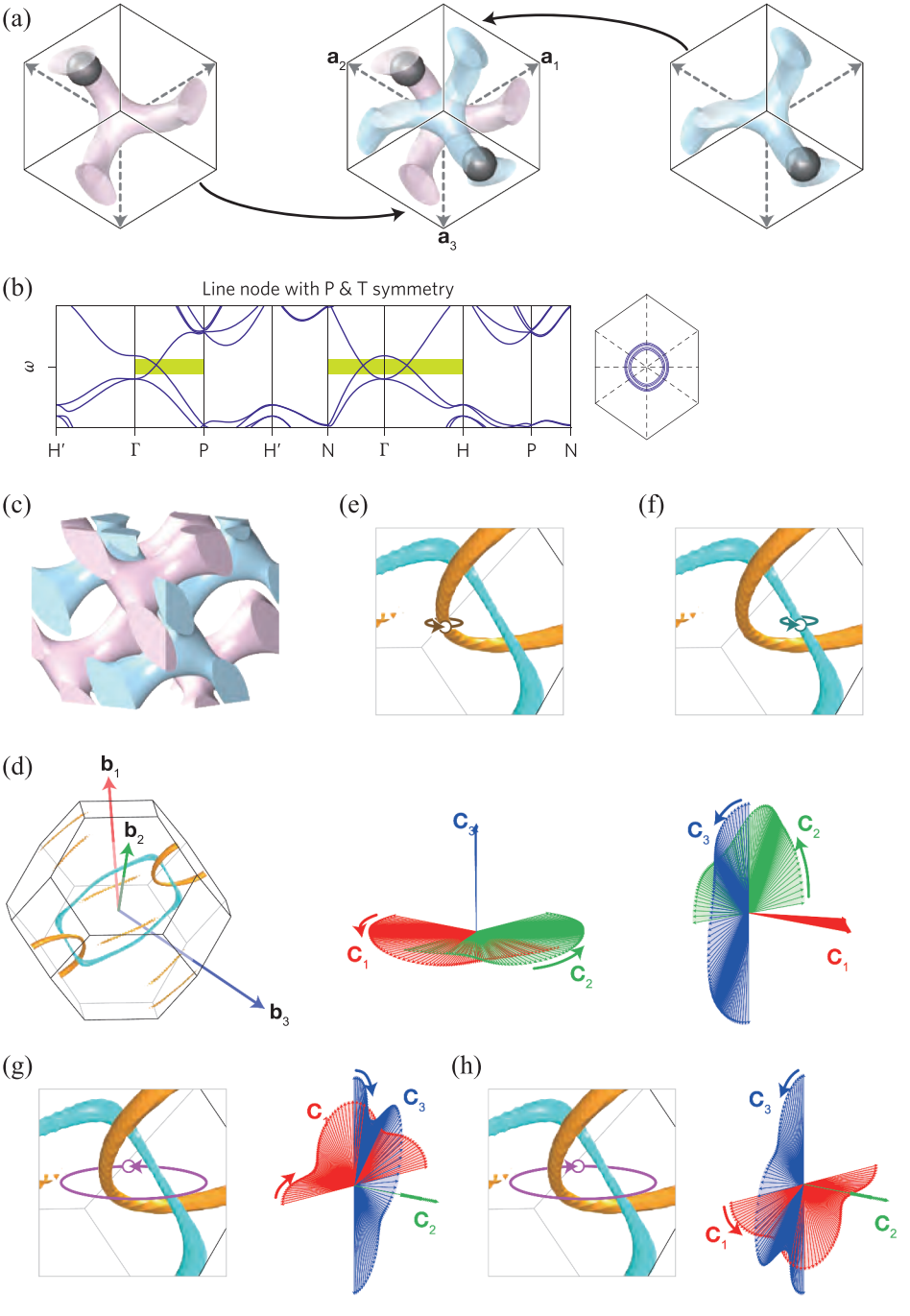

Figure 5. Example of dielectric photonic crystals that exhibit nodal lines in the momentum space. (a) Double gyroid photonic crystal that possesses D_2 symmetry. (b) Photonic band structure of (a) that exhibits a nodal ring (b). Reprinted with permission from ref. [18] copyright 2013 springer nature. (c) Anisotropic double diamond photonic crystal. (d) Nodal link by (c). (e-h) frame rotation charges of (d). Each represents $+\boldsymbol{k}$, $+\boldsymbol{i}$, $-\boldsymbol{j}$, and $+\boldsymbol{j}$, respectively. Upper or left insets of (e-h) also have the enlargements for the sections where the frame rotation charges are calculated. (c-h) are reprinted with permission from ref. [19] copyright 2021 American chemical society.

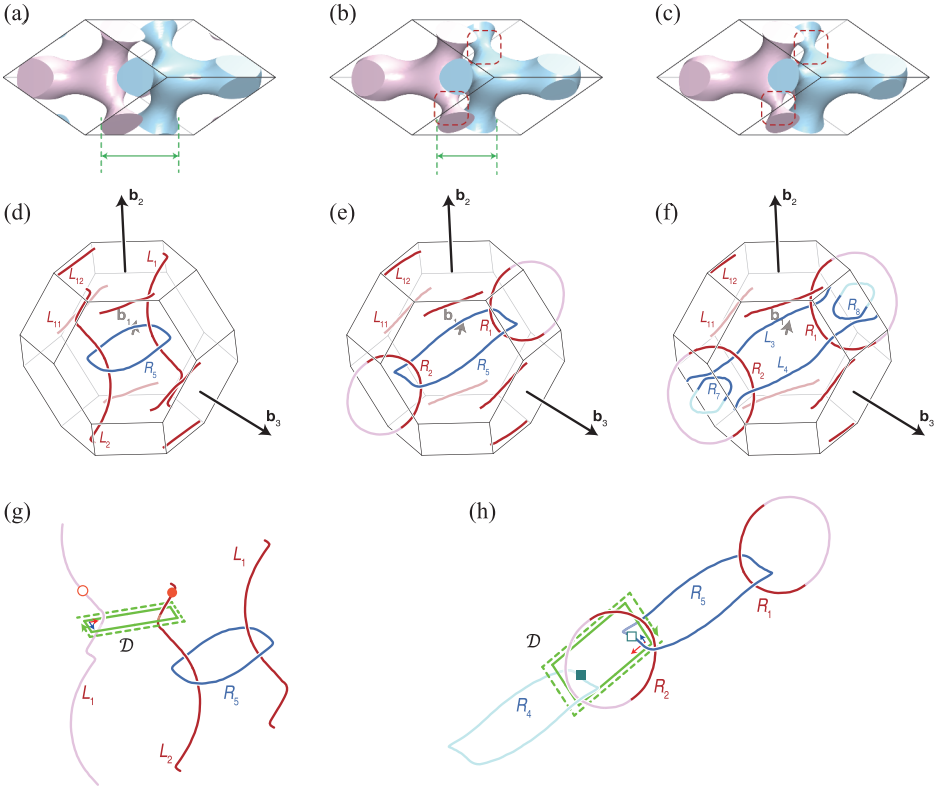

Figure 6. Nodal lines' phase transitions by deforming a dielectric double diamond photonic crystal. (a-c) Three states of the double diamond. The differences between each state are denoted by the green arrows or red dotted boxes. (d-f) Nodal line configurations of (a-c), respectively. (g-h), Extracted nodal lines from (d) and (e), respectively. The planes $\mathcal{D}$ where the Euler class is calculated over are also plotted. All the panels are reprinted with permission from ref. [20] copyright 2024 De Gruyter.

result exhibits the phase transition of the central nodal ring in Figure 6e into the separated nodal rings and nodal lines, as shown in Figure 6f [20].

The Euler class is utilized to analyze the phase transition in Figure 6d–f. The situations in Figure 6g,h are extracted from Figure 6d,e, respectively, and commonly have the plane $\mathcal{D}$ that is pierced by two nodal lines of the same pair of bands. The Euler classes calculated over $\mathcal{D}$ in Figure 6g,h are commonly zero, which means the nodal lines can be pair-annihilated to induce the phase transition. As the Euler class says, the phase transition occurs around the region with the zero Euler class [20].

4. Non-Abelian topology in non-hermitian systems

4.1. Brief introduction of non-hermitian physics

In quantum mechanics, Hamiltonians for energy-conserving systems are Hermitian ($H^\dagger = H$), resulting in zero net energy flows. In other words,

the eigenenergies of Hermitian systems are real, which means that the amplitude of a wave function neither increases nor decreases because the time evolution of the wave function is expressed by $\psi(t) = \psi_0 \exp(-iEt/\hbar)$ and thus simply oscillates in time. In contrast, non-Hermitian systems in general have complex eigenenergies. This was a common belief until Carl Bender in 1998 showed that $\mathcal{PT}$ symmetric non-Hermitian Hamiltonians give real eigenvalues [21]. This work stimulated many interesting new applications in other fields of research including photonics [22]. An intriguing feature of non-Hermitian physics is the presence of exceptional points, which are characteristic points in a parametric space [23,24]. At exceptional points (EPs), the eigenvalue equation, expressed by 2×2 Hamiltonian, becomes defective and thus has a single solution (one eigenvector with one energy eigenvalue) instead of two solutions. EPs have been extensively studied in the field of photonics, as they could provide unprecedented sensitivities [25–30].

As non-Hermitian systems have complex energies, we cannot apply the theory of non-Abelian topological charges and the Euler classes for multiband systems discussed (Sec. 2 and Sec. 3) where real energies are assumed. Furthermore, the extension to complex eigenvalues gives rise to complex shape of bands and degeneracies, making the physics richer and more intriguing but at the same time making it challenging to grasp the physics due to its complexity.

In this section, we first look at the topology of energy bands in non-Hermitian systems. Second, we explain how their topology can be described in terms of the vorticity of EPs and the braid groups. Then, we will discuss how the braid topology is related to non-Abelian properties. Lastly, we review recent works that demonstrate the braiding using photonic systems.

4.2. Description of non-hermitian system

Non-Hermiticity is typically introduced through non-reciprocal hopping terms or gain/loss terms in Hamiltonians. Then, an eigenvalue equation can be formulated using different boundary conditions: periodic boundary conditions (PBCs) for an infinite array of atoms (or resonators for optical structures) and open boundary conditions (OBCs) for a finite array of atoms. With OBCs, the equation allows non-Hermitian skin effects (NHSEs) which localize the wave function at the boundaries. We encourage the readers to see other papers for more details on the skin effects. With PBCs, we build an eigenvalue equation with Bloch Hamiltonian, which means we express the wave function $\psi(x,t) = \psi_0 \exp(ikx - i\omega t)$ where k is the wave vector and ω is the angular frequency given as $E/\hbar$. Here, since the wavevector k is real for PBCs, the angular frequency becomes a complex number.

Table 1. Comparison between Bloch and non-Bloch states.

Property	Bloch states	non-Bloch states
System type	periodic (e.g., crystals)	non-periodic
Wave function	Bloch periodic, $\psi_k(r) = u_k(r)e^{ik\cdot r}$	irregular or localized
Symmetry	discrete translational symmetry	lack of periodicity
Energy bands	well-defined	localized edge states
Momentum	conserved	not conserved

In condensed matter physics, the energy states present in periodic atomic potentials are called Bloch states, where electrons follow a well-defined periodic structure. In non-Hermitian systems, in contrast, the system's eigenstates exhibit non-periodic behaviour having complex values of eigenvalues or complex wave vectors, showing temporally decaying or spatially localized profiles due to non-reciprocal hopping terms or gain/loss terms in its Hamiltonian. This implies that Bloch periodic functions fail to describe non-Hermitian systems, thus one needs to consider non-Bloch eigenstates which are not periodic. Table 1 shows the important distinction between Bloch and non-Bloch states in general. These non-Bloch states can exhibit unique topological features, like exceptional points or non-reciprocal braiding, where the system's non-Hermitian nature leads to novel phenomena not seen in Hermitian systems, such as asymmetric transport [31,32] or unidirectional edge states [33,34].

Bloch states are defined in the first BZ which is the range of the real wavevector k defined by $[-\pi/a, \pi/a]$ for a 1D periodic structure with the lattice constant a. To describe non-Bloch states which has a complex wavevector, a generalized Brillouin zone (GBZ) has been introduced by replacing k with complex wavevector $\tilde{k}$. As we will see in the next section, this allows us to define a non-Bloch winding number for a non-Hermitian system which is a new topological invariant [35].

4.3. Topological invariants of non-hermitian systems

To understand topological properties of bands of non-Hermitian systems, one needs to define topological invariants. In this section, we will explain how topological invariants are defined. Let us start with 2×2 Bloch Hermitian Hamiltonian that describes two energy bands of Su-Schrieffer-Heeger (SSH) model. Then, we will add non-reciprocal hopping terms or gain/loss terms in the Hamiltonian. This can be extended multiband system and can also be applied to momentum space or parameter spaces with a different dimension. More detailed steps can be found in Ref [36,37].

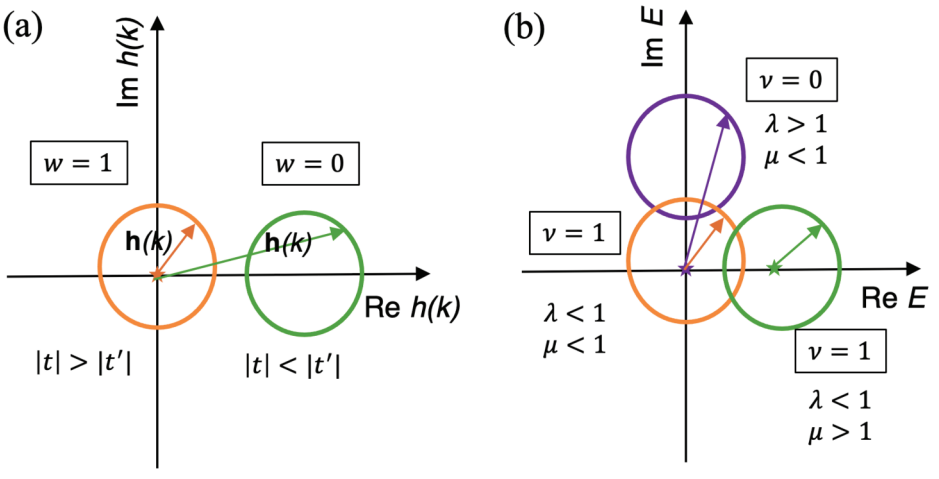

Figure 7. Topological invariants of hermitian and non-hermitian SSH lattices. (a) Winding number w defined with $\mathbf{h}(k)$ in the hermitian SSH Hamiltonian $H = \mathbf{h}(k)\cdot\sigma$ where σ is a vector composed Pauli matrices $(\sigma_x, \sigma_y, \sigma_z)$. (b) The vorticity ν defined in complex energy plane for SSH Hamiltonian with non-hermitian perturbation.

The topological invariant of the Hermitian SSH lattice model is the winding number which means how many times the vector $\mathbf{h}(k)$ in the Hamiltonian $H = \mathbf{h}(k)\cdot\sigma$ encircles the origin as shown in Figure 7a. Here, σ is a vector composed of Pauli matrices. This is equivalent to the Zak phase divided by 2π because the points in the circles correspond to the first BZ and the winding number is the integration of phases along the paths.

To consider the topological invariant non-Hermitian system, we can introduce non-Hermitian perturbation $\mu + i\lambda$ to the non-Hermitian SSH Hamiltonian as in Ref [36]. This leads to complex eigenvalues and the energy spectra with PBC form closed circles as shown in Figure 7b. Here, we define the vorticity ν as a winding number of one energy band in the complex energy plane. The vorticity counts how many times the energy goes around a base point which can be the origin or a point in the real energy axis. Depending on whether the base point is inside the circular path or not, the winding number becomes 0 or 1. Please note that the vorticity w is defined for complex energy spectra because the winding number ν is defined for $h(k)$ which is related to eigenvectors or wave functions.

4.4. Extension to generalized brillouin zone

So far, we have considered the topological invariants defined using Bloch states. However, one can define topological invariants based on non-Bloch states and the generalized Brillouin zone (GBZ). Here, we will follow a recent theoretical work [35] which has revealed that the braid group plays a crucial role in characterizing the topology of non-Hermitian periodic systems,

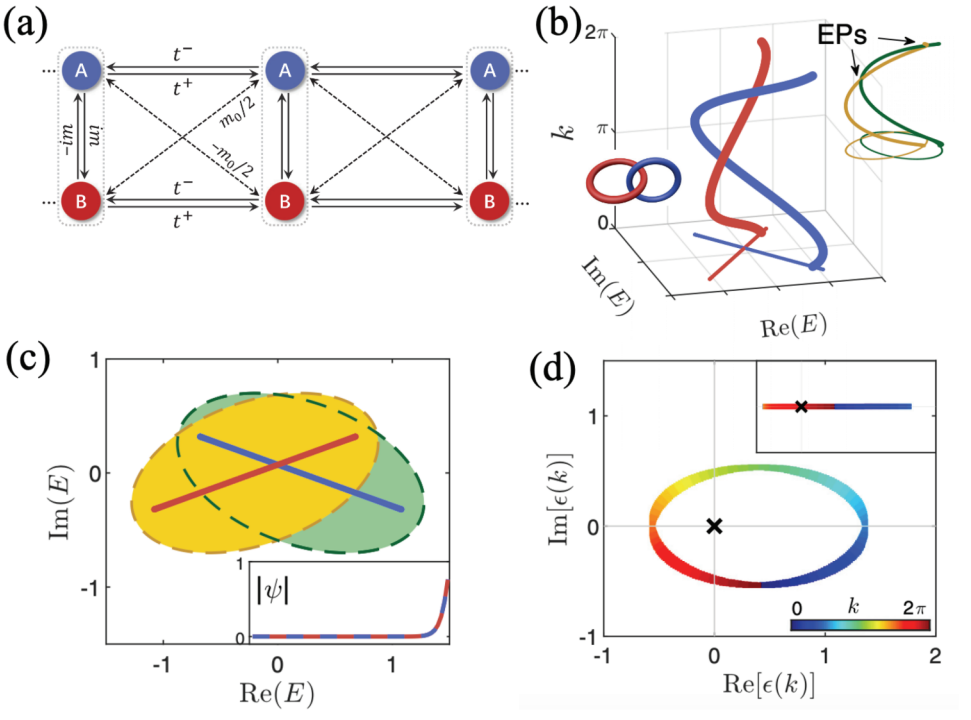

Figure 8. (a) Non-hermitian model with non-reciprocal coupling t^+ and t^- for both sublattices A and B and intersublattice couplings $\pm im$ and $\pm m_0/2$ (b) complex energy spectra $E(k)$ for PBC (green and orange solid lines) and OBC (red and blue solid lines). (c) Projected complex energy spectra PBC (green and orange solid lines) and OBC (red and blue dashed lines) the inset shows a localized mode non-hermitian skin effect with OBC. (d) separation of non-Bloch band $\epsilon(k)$ along the GBZ.

where complex band energies can braid in complex momentum space. Let us consider a tight-binding lattice model that describes non-Hermitian system composed of two sublattices with non-reciprocal couplings ($t^{\pm}$) and intersublattice couplings ($\pm im$ and $\pm m_0/2$) as shown in Figure 8a. The Bloch Hamiltonian can be written as:

$$H(k) = (t\cos k - i\Delta \sin k)\sigma_0 + (m + m_0 \sin k)\sigma_y, \tag{8}$$

where σ_0 is the 2×2 identity matrix, σ_y is the Pauli matrix and k is the real-valued Bloch wave vector. Here, t and Δ are given by the relation $t^{\pm} = (t \pm \Delta)/2$ and non-zero Δ gives non-Hermitian Hamiltonian. Then, the complex eigenenergies under PBC are given by $E_{\pm}(k) = t\cos k - i\Delta \sin k \pm |m + m_0 \sin k|$. As shown in Figure 8b,c, the eigenenergies have the Hopf link topology for PBC and rings with two rings with two intersecting points that correspond to two exceptional points for OBC.

Now, we extend the BZ to the GBZ with the substitution $\beta = e^{i\tilde{k}}$ and complex-valued non-Bloch wave vector $\tilde{k} = k - i \ln r$ to obtain the non-Bloch Hamiltonian $H(\beta)$ from the Bloch Hamiltonian (Eq. 8). The eigenenergies of the non-Bloch bands take the form $E_{\pm}(\beta) = \pm m + 0.5(t - \Delta \mp im_0)\beta + 0.5(t + \Delta \pm im_0)\beta^{-1}$. Because the non-Bloch wave vector includes an imaginary component that governs the localization of bulk eigenstates, the eigenstates are localized on one edge as shown in the inset of Figure 8 showing the NHSE. For this particular system, the GBZ, C_β, is defined with the substitution $\beta = re^{ik}$ for the real part of $\tilde{k}$ (written above), becomes a circle with a radius r, which can be calculated as:

$$r = \sqrt{\left|\frac{(t + \Delta + im_0)}{(t - \Delta - im_0)}\right|}. \tag{9}$$

Then, one can define a non-Bloch winding number W for the non-Bloch bands,

$$W = \frac{1}{2\pi i}\left(\oint_{C_\beta} d \ln \det\left[H(\beta) - \frac{1}{2}\mathrm{Tr}[H(\beta)\right]\right). \tag{10}$$

As shown in Figure 8b, the complex eigenenergies of non-Bloch bands along the GBZ are separable in three-dimensional (E, k)-space, even though they overlap each other in the complex energy plane. The separable non-Bloch band structures show the Hopf link phase and their phases are topologically distinct from a phase where two bands do not braid around each other (the unlink phase not shown here). The non-Bloch winding number W becomes 2 for the Hopf link phases and 0 for the trivial unlink phase. Here, it is clear that the braiding of two energy bands, which also corresponds to Hopf link and unlink, can distinguish the topology of two bands in 1D momentum space. Further, this idea can be extended to the topology of more than two bands in non-Hermitian periodic systems, where complex energies can braid in momentum space [38]. We will look into it in more detail in the following section.

Before that, let us review some work related to the GBZ. We have mentioned the non-Bloch band theory that has been developed for 1D non-Hermitian quantum systems with open boundary conditions (OBC) in Ref. [35], and it also has been verified across various experimental platforms like in electrical and ultracold systems [39–42]. By replacing the conventional BZ, the theory's GBZ accounts for the NHSE and the breakdown of bulk-boundary correspondence [43,44]. Further extensions of this theory have been made to higher dimensions and scale-free localization scenarios (see Ref. [45]). Despite recent work on non-Bloch band topology under

OBC [35], the general definition and properties remain unclear, particularly for generic non-Hermitian systems with multiple non-Bloch bands, each with its own GBZ, referred to as sub-GBZs [15,46,47]. A continuity criterion was proposed in Ref. [48] to separate the sub-GBZs and non-Bloch bands of non-Hermitian multiband quantum systems under OBC. This enabled the construction of their homotopic characterizations, including braiding topology, total vorticity over the OBC bands, and intermediate topological transitions marked by emergent EPs. Please note that these conclusions were demonstrated in a non-Hermitian two-band model meaning they form the Braid group $\mathcal{B}_2$ which is abelian. In the same work, it was found that non-Hermitian open-boundary bands undergo part exchanges when transitioning through specific EPs, a phenomenon also observed in non-Hermitian Bloch bands, previously unidentified. The analysis does not rely on symmetries, though their role in further topological classifications of non-Bloch bands presents an interesting direction for future research.

4.5. Braiding of energy bands

In mathematics, the terms 'braid group' and 'braids' were first coined by Artin in 1925 [49]. The theory of braid group is closely related to knot theory, for example, the non-Abelian group $\mathcal{B}_3$, which considers three stands, is isomorphic to the knot group of the trefoil knot. The mathematical theory of knots has a wide range of applications from physics [50,51] to biology [52]. While the braid group $\mathcal{B}_2$, which considers two strands, is Abelian, the braid groups $\mathcal{B}_n$ can be non-Abelian when the number of strands n is larger than two [53]. This is similar to the BWZ phase and the frame rotation charges described in Chapter 2 which requires multibands to have non-Abelian properties. However, here we consider the braiding of the energy bands in the momentum space or the other parameter spaces instead of the band degeneracies between different bands.

In 2021, K. Wang et al. [54] experimentally demonstrated a tight-binding lattice model capable of realizing an arbitrary number of braiding events involving two energy bands with in a synthetic dimension. The Hamiltonian for this system is expressed in the following form:

$$\begin{aligned} H^{(m)} = \sum_n & g\mathbf{a}_n^\dagger \mathbf{b}_n + g\mathbf{b}_n^\dagger \mathbf{b}_n - i\gamma \mathbf{a}_n^\dagger \mathbf{a}_n + \kappa \mathbf{a}_{n+1}^\dagger \mathbf{a}_n + \kappa \mathbf{a}_n^\dagger \mathbf{a}_{n+1} \\ & + (C-\Delta)\mathbf{a}_{n+m}^\dagger \mathbf{a}_n + (C+\Delta)\mathbf{a}_n^\dagger \mathbf{a}_{n+m}, \end{aligned} \tag{11}$$

where $\mathbf{a}_n^\dagger(\mathbf{a}_n)$ and $\mathbf{b}_n^\dagger(\mathbf{b}_n)$ denote the creation (annihilation) operators of the n-th lattice site in sublattices a and b, respectively. The parameters $\kappa, g, C \pm \Delta \in \mathbb{R}$ denote coupling constants, and and $\gamma > 0$ represents the additional loss rate in sublattice a, exceeding the loss rate in sublattice b. This model includes

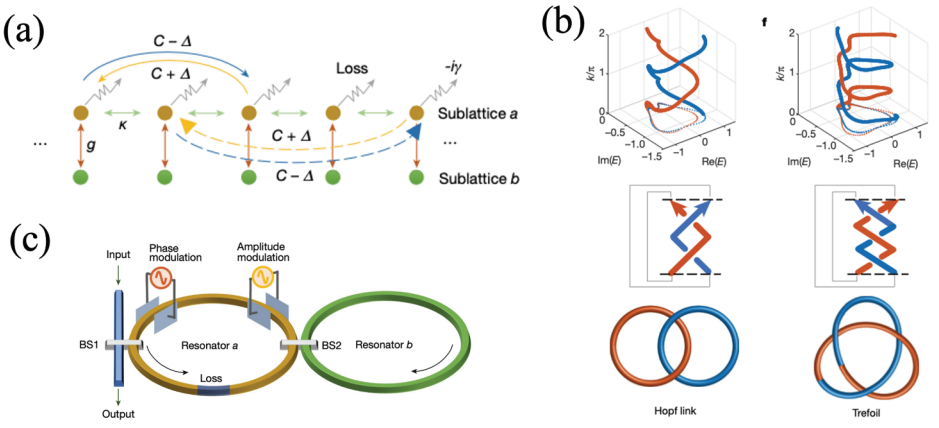

Figure 9. Braiding of two bands in synthetic dimension (a) tight-binding model with first-nearest coupling and second-nearest coupling (needs to be checked). (b) Energy braiding for second-order coupling $m = 2$ (left) and third order coupling $m = 3$ (right) corresponding to Hopf link and trefoil respectively. (c) Schematic of experimental setup with two coupled ring resonators and phase and amplitude modulator to control the coupling between different resonance frequencies which are used for a lattice in the synthetic dimension.

nearest-neighbor coupling, as well as coupling between the m-th neighbors within sublattice a, as shown in Figure 9a. No coupling exists between the sites on sublattice b.

The braiding of the two non-Hermitian bands shown in Figure 9b gives a typical description of braiding in non-Hermitian systems with first and higher-order couplings with different m. To experimentally demonstrate the braiding of two energy bands, they used two coupled ring resonators along with a phase modulator and an amplitude modulator (see Figure 9c), which allows for an 1D periodic lattice in the frequency domain with the designed coupling coefficients.

4.6. Non-Hermitian nodal-line semimetals

In Section 3, we introduced non-Abelian topological charges of multiple bands in multigap systems in three-dimensional momentum space which have real eigenvalues with line degeneracies (nodal lines and nodal rings) due to the $\mathcal{PT}$ symmetry. Recently, Wang et al. [55] showed that a non-Hermitian perturbation, i.e. gain-and-loss perturbation, can split one nodal ring into two exceptional rings (ERs), and, with increasing perturbation strength, some of the ERs may shrink and eventually vanish. Through dimensional reduction, two distinct topological numbers, the vorticity and the winding numbers, were defined to describe the topology of the bulk bands. By comparing the band structures under periodic boundary conditions (PBCs) and open

boundary conditions (OBCs), they find that the conventional bulk-surface correspondence in nodal-line semimetals breaks down in the non-Hermitian case.

Yang et al. [56] proposed a simple method to realize Hopf link exceptional line (EL) semimetals by applying non-Hermitian perturbations to nodal-line semimetals. The Fermi surfaces (FSs) of the Hopf-link EL semimetals exhibit a twisting structure, with the boundaries forming a Hopf link. The linking number is constructed from a dual Hermitian Hamiltonian, whose nodal lines share the same topology as the ELs. The authors show that the Hopf-link phase is robust and can be characterized by the winding number of the non-Hermitian perturbations along the nodal line.

The main assumption in these works is that the momentum space is kept real but the energy eigenvalues change from real numbers to complex number allowing for an exceptional point which divides two regimes of purely real or purely imaginary energy eigenvalues. Finite systems with those gain-loss perturbations, modeled by the lattice with the OBC, can support an edge mode localized at the boundary due to the NHSE.

In 2021, Ezawa [45] proposed a non-Hermitian non-Abelian topological insulator using a two-band model in one dimension by imposing $\mathcal{PT}$ symmetry. In the Hermitian limit, the two-band model describes a real-line-gap topological insulator with real eigenvalues. However, as the non-Hermitian term increases, the system undergoes $\mathcal{PT}$ symmetry breaking and makes a transition into an imaginary-line-gap topological insulator with flat bulk bands. Specifically, by introducing a bulk-bending term, the author demonstrated two phase transitions, leading to a metallic phase with complex eigenvalues. With a circuit model, he also showed that these models can be realized in electric circuits, where $\mathcal{PT}$ symmetry breaking and topological edge states can be detected by measuring impedance resonance.

4.7. Photonic non-abelian braid monopole

Monopoles and braids represent fascinating yet elusive features in the fundamental theories of light and matter. For example, in lattice field theory, monopoles associated with band-structure degeneracies are governed by the well-known no-go (Fermion doubling) theorem [57,58]. According to the no-go theorem, the charges carried by particles are generally balanced by their counterparts, thereby preventing the formation of monopoles. This principle is believed to hold universally, applying to both closed Hermitian systems and open non-Hermitian systems. Recently, Wang et al. [59] showed that the traditional form of this theorem does not apply to non-Abelian charges hence non-Abelian braid topology in non-Hermitian multi-band systems offers a

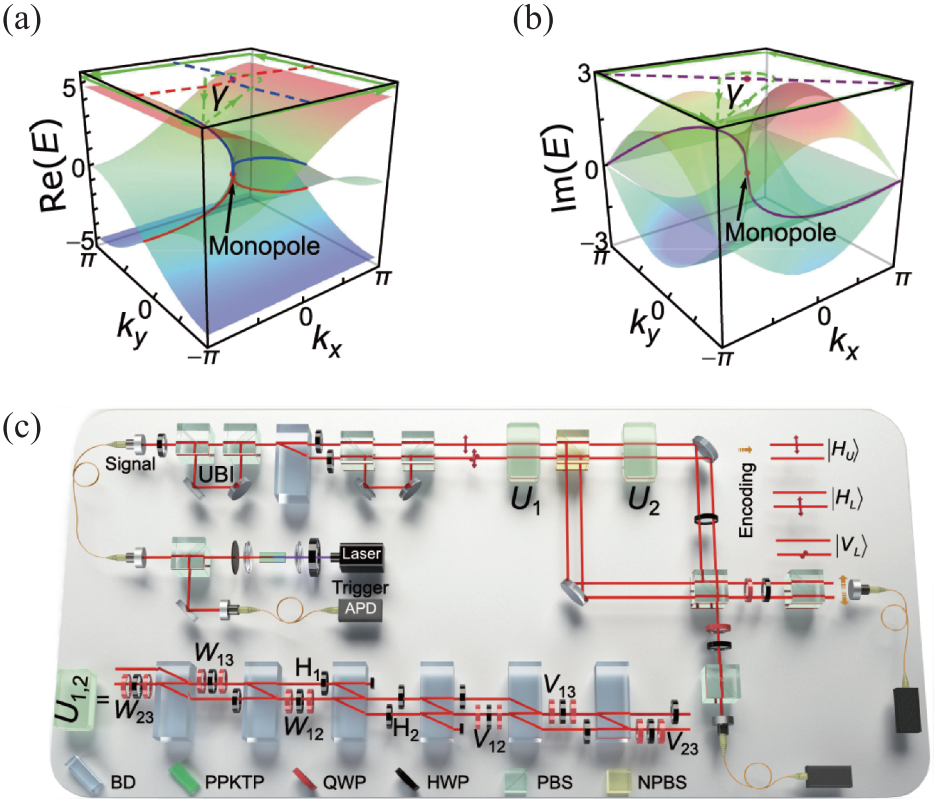

Figure 10. Theoretical results for (a) real and (b) imaginary parts of the spectrum. The red dot marks the non-abelian monopole. The solid lines depict the fermi arcs of the real spectral components and the i-fermi arcs of the imaginary components, respectively. The dashed lines are their projections onto the k_x-k_y plane. The path γ encircles the monopole and has $k_x = k_y = -\pi$ as its base point. (c) Experimental setup for the observation of the non-abelian monopole. Generate photon pairs, consisting of trigger and signal photon, via type-II spontaneous parametric down-conversion through a periodically poled potassium titanyl phosphate (PPKTP) crystal. Reprinted from ref. [59].

striking exception by creating monopoles, as shown in Figure 10a,b. They exploit this exception and, for the first time, experimentally realize a monopole degeneracy in a non-Hermitian three-band system, manifesting as a single third-order exceptional point.

To experimentally implement the non-Abelian monopoles, one needs a dissipative system which is non-Hermitian. Band crossings in such systems are generically two-fold exceptional points (EP2s) [60,61]. The non-Abelian nature of these EP2s emerges from the complex-valued 'energies', which reflect the dissipation inherent in the underlying systems. These energies braid around each other near the EP2s, assigning a braid topological invariant to each of them. As we briefly mentioned in Section 4.5, these braids become non-Abelian for systems with more than two bands [5,54,62], enabling the possibility of bypassing fermion-doubling constraints and constructing

braid-protected monopoles in multi-band dissipative systems [39]. While dissipation is a common feature in photonic, mechanical, and electrical circuit systems, the observation and manipulation of monopoles and non-Abelian phenomena remain challenging due to the lack of a suitably tunable dissipative system.

In Ref. [59], the authors report the experimental creation and manipulation of a non-Abelian monopole and EP2s within a single-photon interferometric network Figure 10c, where they control and observe the EP2s, which either results in gap-opening or a non-Abelian monopole depending on the topology of their preceding paths. They further demonstrate that non-Hermitian phase transitions are induced by the movement of EP2s along these paths, providing clear evidence of the non-Abelian nature of the setup. Unlike non-Abelian phenomena in many-body systems or Hermitian non-interacting systems, their setup does not rely on finely tuned interactions or additional symmetries. Instead, it capitalizes on the topological robustness of braids.

5. Non-Abelian holonomy in coupled optical waveguides

As we have seen so far, the introduction of non-Abelian topological charges of multiple photonic bands gives us useful insight on the pair creation and annihilation of bands. To consider this non-Abelian band topology, we have considered three-dimensional structures because the nodal lines are present in three-dimensional momentum space. However, we can relax this constraint by having one extra dimension coming from the time or frequency in two-dimensional structures. In optics, for example, the non-Abelian property (non-commutativity) can be observed for two-dimensional array of coupled optical waveguide where the propagation direction is considered as one extra dimension. Indeed, an array of coupled optical waveguides has been an excellent platform for experimental demonstration of the topological effects of photons, for example, edge states in photonic graphene [63]. Further, we can consider non-Abelian holonomy of optical propagation in a finite number of waveguide arrays which do not have periodicity in any direction but the optical modes transform while propagating along the waveguides due to a modulated coupling coefficients. In this section, we will review recent work on non-Abelian effects in optical systems which uses optical waveguide.

In 2019, Kremer et al. demonstrated non-Abelian holonomy with coupled waveguides where they considered geometric phases of the symmetry group U(2) and U(3) [64]. More recently, V. Neef et al. employed an experimental setup made of coupled waveguides to realize non-Abelian quantum holonomy of the symmetry group U(3) with closed path in the parameters space

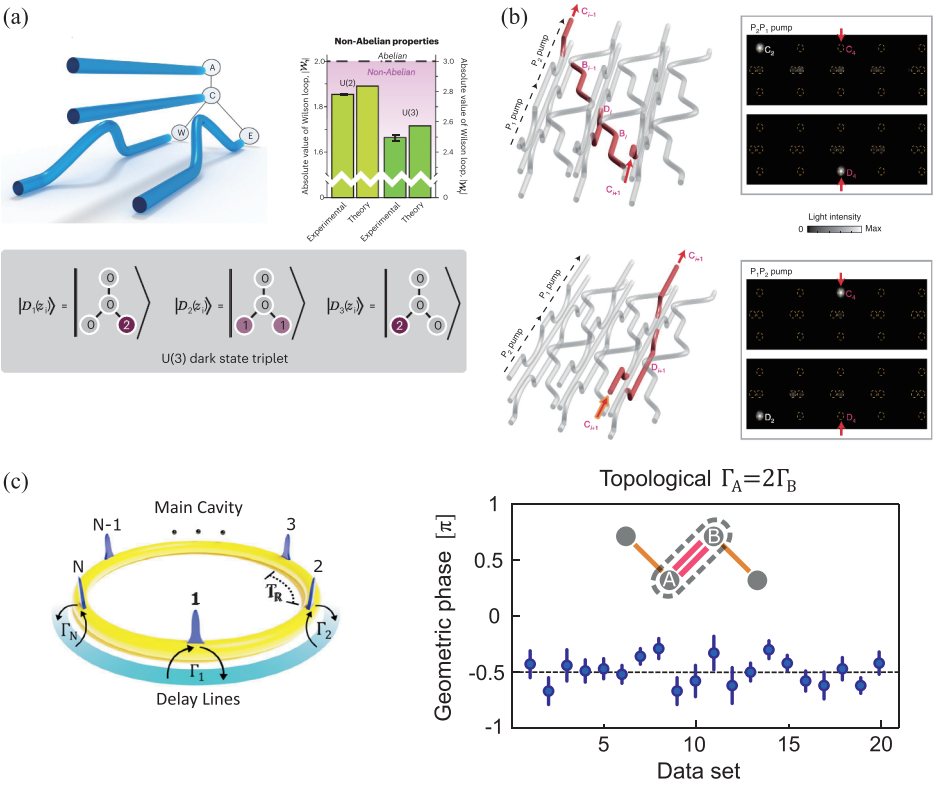

Figure 11. (a) Non-abelian holonomy in coupled waveguides. Reprinted with permission from ref. [4] copyright 2022 springer nature. (b) Non-abelian transport using thouless pumping. Reprinted with permission from ref. [65] copyright 2022 springer nature. (c) Non-abelian dissipative coupling. Reprinted with permission from ref. [66] copyright 2023 springer nature.

composed of the coupling coefficients [4]. As shown in Figure 11a, the coupling coefficients vary along the propagation direction while the input port (front) and output port (back) have the same geometry with the three identical coupling coefficients making the initial and final states of photons defined based on the U(3) dark state triplets. Then, the absolute value of Wilson loop for the optical path becomes non-integer proving the adiabatic change is non-Abelian. Interestingly, they used indistinguishable photons to show that the same concept works for photons demonstrating the non-Abelian quantum holonomy.

The idea of holonomy with adiabatic change can be applied to a one-dimensional periodic optical waveguide array with periodic modulation of coupling in the propagation direction. This kind of optical systems implements the Thouless pumping for photons and the process becomes non-Abelian, similarly to the quantum holonomy with four coupled waveguides [67]. Recently, non-Abelian Thouless pumping has been shown experimentally using photonic waveguides in the Lieb lattice, as shown in Figure 11b [65].

Parto et al. [66] recently demonstrated non-Abelian effects in non-Hermitian systems with dissipative couplings. They have implemented the dissipatively coupled resonators using time-multiplexed photonic optical cavities. Then they compared the experimental results with theoretical calculations based on the Lindblad equation and matrix-valued modified Wilson lines (see Figure 11c).

6. Summary and outlook

In summary, we have introduced the basic concepts of non-Abelian topological charges of nodal lines in the three-dimensional momentum space and have reviewed the recent numerical and experimental demonstration of these non-Abelian nodal lines using three-dimensional periodic structures such as metamaterials and photonic crystals. Indeed, the identification of non-Abelian topological charges using the frame rotation charges represented by quaternion numbers or the Euler class allows us to judge the stability of nodal lines, proving that they are very important mathematical values for the analysis of multigap topology. Then, we reviewed recent theoretical efforts to study non-Abelian nature in non-Hermitian systems, which may not have periodic Bloch modes but instead localized modes called non-Bloch modes due to non-reciprocal couplings and gain/loss inclusion. The energy spectrum in different number of band systems has been analyzed in complex frequency – real wavevector space showing braiding of the bands and also in real frequency and complex wavevector space where the solutions become non-Bloch modes. Finally, we looked at the non-Abelian holonomy in both a finite number of coupled optical waveguides and one-dimensional periodic waveguides. The modulated coupling approach shows the possibility of applying the non-Abelian holonomy to quantum optics and also using Thouless pumping to control the photon propagation.

The use of the non-Abelian group for topological invariants allows us to describe the topology of multigap systems. As we have seen so far, for the last decade, the theory of non-Abelian groups has accelerated the study of intriguing and rich physics in photonic systems. Although there remain many challenges and unanswered questions, for example, what would be the directly observable physical consequence of having non-Abelian topological charges? Also, most of the study on non-Abelian topological charges in non-Hermitian systems remains at the stage of theoretical model. Nevertheless, we believe there will be interesting experimental demonstrations using active optical systems such as lasers or optical ring resonators with amplitude and phase modulators. Also, acoustic metamaterial could be a good system to show the non-Abelian topology in non-Hermitian system due to its simplicity of defining structures and measurements. With the promising development

on this topic, we believe that the theoretical study summarized in this review will be a strong building block for future research.

Disclosure statement

No potential conflict of interest was reported by the author(s).

References

[1] Wu QS, Soluyanov AA, Bzdušek T. Non-Abelian band topology in noninteracting metals. Science. 2019;365:1273–1277. doi: 10.1126/science.aau8740

[2] Park H, Lee S. Double gyroids for frequency-isolated Weyl points in the visible regime and interference lithographic design. ACS Photon. 2020;7:1577–1585. doi: 10.1021/acsphotonics.0c00532

[3] Park H, Gao W, Zhang X, et al. Nodal lines in momentum space: topological invariants and recent realizations in photonic and other systems. Nanophoton. 2022 Jun;11:2779–2801. doi: 10.1515/nanoph-2021-0692

[4] Neef V, Pinske J, Klauck F, et al. Three-dimensional non-abelian quantum holonomy. Nat Phys. 2022 Dec;19:30–34. doi: 10.1038/s41567-022-01807-5

[5] Li Z, Mong RSK. Homotopical characterization of non-hermitian band structures. Phys Rev B. 2021 Apr;103:155129. doi: 10.1103/PhysRevB.103.155129

[6] Yang Y, Yang B, Ma G, et al. Non-Abelian physics in light and sound. Science. 2024 Feb;383:eadf9621. doi: 10.1126/science.adf9621

[7] Park H, Wong S, Bouhon A, et al. Topological phase transitions of non-abelian charged nodal lines in spring-mass systems. Phys Rev B. 2022 Jun;105:214108. doi: 10.1103/PhysRevB.105.214108

[8] Berry MV. Quantal phase factors accompanying adiabatic changes. Proceedings of the Royal Society of London. A. Mathematical and Physical Sciences. 1984;392:45–57.

[9] Wilczek F, Zee A. Appearance of gauge structure in simple dynamical systems. Phys Rev Lett. 1984;52:2111–2114. doi: 10.1103/PhysRevLett.52.2111

[10] Tiwari A, Bzdusek T. Non-abelian topology of nodal-line rings in PT -symmetric systems. Phys Rev B. 2020 May;101:195130. doi: 10.1103/PhysRevB.101.195130

[11] Park H, Oh SS. Sign freedom of non-abelian topological charges in phononic and photonic topological semimetals. New J Phys. 2022 May;24:053042. doi: 10.1088/1367-2630/ac6ca3

[12] Bouhon A, Wu Q, Slager R-J, et al. Non-abelian reciprocal braiding of Weyl points and its manifestation in zrte. Nat Phys. 2020;16:1137–1143. doi: 10.1038/s41567-020-0967-9

[13] Gao W, Yang B, Tremain B, et al. Experimental observation of photonic nodal line degeneracies in metacrystals. Nat Commun. 2018;9:950. doi: 10.1038/s41467-018-03407-5

[14] Yan Q, Liu R, Yan Z, et al. Experimental discovery of nodal chains. Nat Phys. 2018;14:461–464. doi: 10.1038/s41567-017-0041-4

[15] Yang Z, Zhang K, Fang C, et al. Non-hermitian bulk-boundary correspondence and auxiliary generalized brillouin zone theory. Phys Rev Lett. 2020 Nov 27;125:226402. doi: 10.1103/PhysRevLett.125.226402

[16] Wang D, Wu Y, Zhang ZQ, et al. Non-abelian frame charge flow in photonic media. Phys Rev X. 2023 May;13:021024. doi: 10.1103/PhysRevX.13.021024

[17] Wang D, Yang B, Wang M, et al. Observation of non-abelian charged nodes linking nonadjacent gaps. Phys Rev Lett. 2022 Dec;129:263604. doi: 10.1103/PhysRevLett.129.263604

[18] Lu L, Fu L, Joannopoulos JD, et al. Weyl points and line nodes in gyroid photonic crystals. Nat Photon. 2013 Apr;7:294–299. doi: 10.1038/nphoton.2013.42
[19] Park H, Wong S, Zhang X, et al. Non-abelian charged nodal links in a dielectric photonic crystal. ACS Photonics. 2021;8:2746–2754. doi: 10.1021/acsphotonics.1c00876
[20] Park H, Jones A, Kim M, et al. Topological phase transition and surface states in a non-abelian charged nodal line photonic crystal. Nanophotonics. 2024;13:1079–1089. doi: 10.1515/nanoph-2023-0906
[21] Bender CM, Boettcher S. Real spectra in non-hermitian hamiltonians having PT symmetry. Phys Rev Lett. 1998;80:5243. doi: 10.1103/PhysRevLett.80.5243
[22] Peng B, Özdemir ŞK, Lei F, et al. Parity–time-symmetric whispering-gallery microcavities. Nat Phys. 2014 Apr 6;10:394–398. doi: 10.1038/nphys2927
[23] Regensburger A, Bersch C, Miri M-A, et al. Parity–time synthetic photonic lattices. Nature. 2012;488:167–171. doi: 10.1038/nature11298
[24] Özdemir ŞK, Rotter S, Nori F, et al. Parity–time symmetry and exceptional points in photonics. Nat Mater. 2019 Aug;18:783–798. doi: 10.1038/s41563-019-0304-9
[25] Hodaei H, Miri M-A, Heinrich M, et al. Parity-time – symmetric microring lasers. Science. 2014;346:975. doi: 10.1126/science.1258480
[26] Wiersig J. Enhancing the sensitivity of frequency and energy splitting detection by using exceptional points: application to microcavity sensors for single-particle detection. Phys Rev Lett. 2014;112:203901. doi: 10.1103/PhysRevLett.112.203901
[27] Chen W, Özdemir ŞK, Zhao G, et al. Exceptional points enhance sensing in an optical microcavity. Nature. 2017;548:192–196. doi: 10.1038/nature23281
[28] Langbein W. No exceptional precision of exceptional-point sensors. Phys Rev A. 2018;98:023805. doi: 10.1103/PhysRevA.98.023805
[29] Makris KG. Transient growth and dissipative exceptional points. Phys Rev E. 2021 Nov;104:054218. doi: 10.1103/PhysRevE.104.054218
[30] Peng B, Bouhon A, Monserrat B, et al. Phonons as a platform for non-abelian braiding and its manifestation in layered silicates. Nat Commun. 2022;13:423. doi: 10.1038/s41467-022-28046-9
[31] Longhi S. Non-hermitian bidirectional robust transport. Phys Rev B. 2017 Jan;95:014201. doi: 10.1103/PhysRevB.95.014201
[32] Longhi S, Gatti D, Valle GD. Robust light transport in non-hermitian photonic lattices. Sci Rep. 2015 Aug;5:13376. doi: 10.1038/srep13376
[33] Jin L. Topological phases and edge states in a non-hermitian trimerized optical lattice. Phys Rev A. 2017 Sep;96:032103. doi: 10.1103/PhysRevA.96.032103
[34] Gao P, Willatzen M, Christensen J. Anomalous topological edge states in non-hermitian piezophononic media. Phys Rev Lett. 2020 Nov;125:206402. doi: 10.1103/PhysRevLett.125.206402
[35] Li Y, Ji X, Chen Y, et al. Topological energy braiding of non-Bloch bands. Phys Rev B. 2022 Nov;106:195425. doi: 10.1103/PhysRevB.106.195425
[36] Ghatak A, Das T. New topological invariants in non-hermitian systems. J Phys: Condens Matter. 2019 July 3;31:263001. doi: 10.1088/1361-648X/ab11b3
[37] Ryu J-W, Han J-H, Yi C-H, et al. Exceptional classifications of non-hermitian systems. Commun Phys. 2024;7:109. doi: 10.1038/s42005-024-01595-9
[38] Wojcik CC, Sun X-Q, Bzdušek TCV, et al. Homotopy characterization of non-hermitian hamiltonians. Phys Rev B. 2020 May;101:205417. doi: 10.1103/PhysRevB.101.205417
[39] König JLK, Yang K, Budich JC, et al. Braid-protected topological band structures with unpaired exceptional points. Phys Rev Res. 2023 Oct;5:L042010. doi: 10.1103/PhysRevResearch.5.L042010

[40] Xiao L, Deng T, Wang K, et al. Non-hermitian bulk–boundary correspondence in quantum dynamics. Nat Phys. 2020 Jul;16:761–766. doi: 10.1038/s41567-020-0836-6
[41] Stegmaier A, Imhof S, Helbig T, et al. Topological defect engineering and P T symmetry in non-hermitian electrical circuits. Phys Rev Lett. 2021 May;126:215302. doi: 10.1103/PhysRevLett.126.215302
[42] Helbig T, Hofmann T, Imhof S, et al. Generalized bulk–boundary correspondence in non-hermitian topolectrical circuits. Nat Phys. 2020 Jul;16:747–750. doi: 10.1038/s41567-020-0922-9
[43] Hasan MZ, Kane CL. Colloquium: topological insulators. Rev Mod Phys. 2010 Nov;82:3045–3067. doi: 10.1103/RevModPhys.82.3045
[44] Qi X-L, Zhang S-C. Topological insulators and superconductors. Rev Mod Phys. 2011 Oct;83:1057–1110. doi: 10.1103/RevModPhys.83.1057
[45] Ezawa M. Non-hermitian non-abelian topological insulators with PT symmetry. Phys Rev Res. 2021 Oct;3:043006. doi: 10.1103/PhysRevResearch.3.043006
[46] Fu Y, Wan S. Degeneracy and defectiveness in non-hermitian systems with open boundary. Phys Rev B. 2022 Feb;105:075420. doi: 10.1103/PhysRevB.105.075420
[47] Fu Y, Zhang Y. Anatomy of open-boundary bulk in multiband non-hermitian systems. Phys Rev B. 2023 Mar;107:115412. doi: 10.1103/PhysRevB.107.115412
[48] Fu Y, Zhang Y. Braiding topology of non-hermitian open-boundary bands. Phys Rev B. 2024 Sep;110:L121401. doi: 10.1103/PhysRevB.110.L121401
[49] Magnus W. Braid groups: a survey. Proceedings of the Second International Conference on the Theory of Groups. 1974;372:463–487.
[50] Leach J, Dennis MR, Courtial J, et al. Knotted threads of darkness. Nature. 2004 Nov;432:165–165. doi: 10.1038/432165a
[51] Kedia H, Bialynicki-Birula I, Peralta-Salas D, et al. Tying knots in light fields. Phys Rev Lett. 2013 Oct;111:150404. doi: 10.1103/PhysRevLett.111.150404
[52] Shimokawa K, Ishihara K, Grainge I, et al. FtsK-dependent XerCD-dif recombination unlinks replication catenanes in a stepwise manner. Proc Natl Acad Sci USA. 2013 Dec 24;110:20906–20911. doi: 10.1073/pnas.1308450110
[53] Artin E. Theory of braids. The Ann Of Math. 1947;48:101–126. doi: 10.2307/1969218
[54] Wang K, Dutt A, Wojcik CC, et al. Topological complex-energy braiding of non-hermitian bands. Nature. 2021 Oct;598:59–64. doi: 10.1038/s41586-021-03848-x
[55] Wang H, Ruan J, Zhang H. Non-hermitian nodal-line semimetals with an anomalous bulk-boundary correspondence. Phys Rev B. 2019 Feb;99:075130. doi: 10.1103/PhysRevB.99.075130
[56] Yang Z, Hu J. Non-hermitian hopf-link exceptional line semimetals. Phys Rev B. 2019 Feb;99:081102. doi: 10.1103/PhysRevB.99.081102
[57] Nielsen H, Ninomiya M. Absence of neutrinos on a lattice: (i). proof by homotopy theory. Nucl Phys B. 1981;185:20–40. doi: 10.1016/0550-3213(81)90361-8
[58] Nielsen H, Ninomiya M. Absence of neutrinos on a lattice: (ii). intuitive topological proof. Nucl Phys B. 1981;193:173–194. doi: 10.1016/0550-3213(81)90524-1
[59] Wang K, König JLK, Yang K, etal. Photonic non-abelian braid monopole. arXiv [cond-matmes-hall]. 2024;2410:08191.
[60] Berry MV. Physics of nonhermitian degeneracies. Czech J Phys. 2004 Oct;54:1039–1047. doi: 10.1023/B:CJOP.0000044002.05657.04
[61] Heiss WD. The physics of exceptional points. J Phys A: Math Theor. 2012 oct;45:444016. doi: 10.1088/1751-8113/45/44/444016
[62] Hu H, Zhao E. Knots and non-hermitian Bloch bands. Phys Rev Lett. 2021 Jan;126:010401. doi: 10.1103/PhysRevLett.126.010401

[63] Plotnik Y, Rechtsman MC, Song D, et al. Observation of unconventional edge states in 'photonic graphene'. Nat Mater. 2014;13:57–62.
[64] Kremer M, Teuber L, Szameit A, et al. Optimal design strategy for non-abelian geometric phases using abelian gauge fields based on quantum metric. Phys Rev Res. 2019 Nov 20;1:033117. doi: 10.1103/PhysRevResearch.1.033117
[65] Sun Y-K, Zhang X-L, Yu F, et al. Non-abelian thouless pumping in photonic waveguides. Nat Phys. 2022 July;18:1080–1085. doi: 10.1038/s41567-022-01669-x
[66] Parto M, Leefmans C, Williams J, et al. Non-abelian effects in dissipative photonic topological lattices. Nat Commun. 2023 Mar;14:1440. doi: 10.1038/s41467-023-37065-z
[67] Brosco V, Pilozzi L, Fazio R, et al. Non-abelian thouless pumping in a photonic lattice. Phys Rev A. 2021 Jun 24;103:063518. doi: 10.1103/PhysRevA.103.063518